

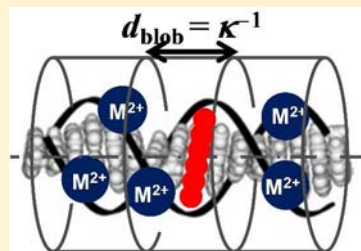
Lateral Distribution of Charged Species along a Polyelectrolyte Probed with a Fluorescence Blob Model

Christine Keyes-Baig, Manoj Mathew, and Jean Duhamel*

Institute of Polymer Research, Waterloo Institute of Nanotechnology, Department of Chemistry, University of Waterloo, Waterloo, ON, Canada N2L 3G1

Supporting Information

ABSTRACT: The distribution of metal counterions binding onto the oppositely charged surface of a model polyelectrolyte, namely, DNA, was characterized by conducting fluorescence quenching experiments. In these experiments, DNA was used as a molecular ruler to measure the average distance (d_{blob}) over which electron transfer takes place between DNA-intercalated ethidium bromide (DNA-EB) and the electrostatically bound divalent metal cations Ni^{2+} and Cu^{2+} . Analysis of the fluorescence decays of DNA-EB quenched by Cu^{2+} and Ni^{2+} with the fluorescence blob model showed that d_{blob} was equal to the Debye length (κ^{-1}). This surprisingly simple result considering the overall complexity of the system under study led to the straightforward proposal that counterions bind to a polyelectrolyte by distributing themselves randomly into an array of self-defined subdomains of dimension κ^{-1} . In turn, this insight can be utilized to rationalize the complex behavior of polyelectrolytes in aqueous solution.



INTRODUCTION

Strong, long-range electrostatic forces impart polyelectrolytes with unique properties that are harvested by nature and humankind in a bewildering array of applications. The compaction of meter-long chromosomal DNA into a chromosome territory in the cell nucleus of only a few micrometers in diameter,¹ the self-association of DNA with cationic surfactants into lipoplexes used for gene delivery,² the layer-by-layer deposition of polyelectrolytes bearing opposite charges to create novel sensors,³ and the alternate reduction and oxidation of polyelectrolytes to generate the actuating parts of micrometer-sized robots⁴ are all examples of applications resulting from strong electrostatic interactions with polyelectrolytes. Because of their importance in numerous areas of science, the characterization of the electrostatic forces induced by polyelectrolytes and their effect on the surrounding population of oppositely charged species has been and continues to be the focus of intense research, as a number of recent reviews attest.^{5–9}

Since many of the applications involving polyelectrolytes revolve around the massive compaction experienced by the polyelectrolyte upon its condensation with counterions, numerous theoretical and experimental studies have aimed at defining the conditions that lead to condensation.^{5–9} These conditions are typically obtained by considering the electrostatic potential $\psi(r)$ generated by the polyelectrolyte to which the counterions located at a distance r away from the axis but still in the vicinity of the polyelectrolyte are subjected. Application of the Poisson–Boltzmann approximation yields a $\psi(r)$ that decays more or less exponentially with the distance r away from the main axis of the closed surface defined by the polyelectrolyte charges and becomes negligible for distances $r \geq$

$5\kappa^{-1}$, where κ^{-1} is the Debye length.⁶ Over 40 years ago,^{10–12} Manning successfully applied these theoretical procedures to predict the fraction of polyelectrolyte charges that are neutralized by counterions in solution,¹³ and these procedures continue to be improved to provide better characterizations of the effective charge of a polyelectrolyte.^{14,15} These procedures have been exploited to provide a detailed description of $\psi(r_o, z)$, where r_o and z represent the distances corresponding to the locations at and along the main axis of the polyelectrolyte surface, respectively.¹⁶ More recently, the condensation of counterions into discrete periodic arrays along the DNA helix has been demonstrated mathematically^{17,18} for dense systems involving close-range interactions between DNA helices to rationalize the collapse of polyelectrolytes in the presence of counterions¹⁹ and the attractive DNA–DNA interactions that are observed in DNA aggregates²⁰ and dense lipoplex complexes of DNA and cationic lipid membranes.²¹ In the case of DNA helices in dilute solution, a schematic representation of $\psi(r)$ is given in Figure 1A using DNA as a model polyelectrolyte, while the interactions between counterions subject to $\psi(r_o, z)$ are schematically depicted in Figure 1B. The $\psi(r_o, z)$ profile along the main axis of the polyelectrolyte surface can be used to describe the spatial distribution, correlations, and dynamics of counterions at the polyelectrolyte surface, which have been recognized as being extremely important to rationalize the behavior of polyelectrolytes.⁵ For instance, such considerations were invoked to explain the formation of counterion charge density waves at the surface of

Received: July 26, 2012

Published: September 17, 2012

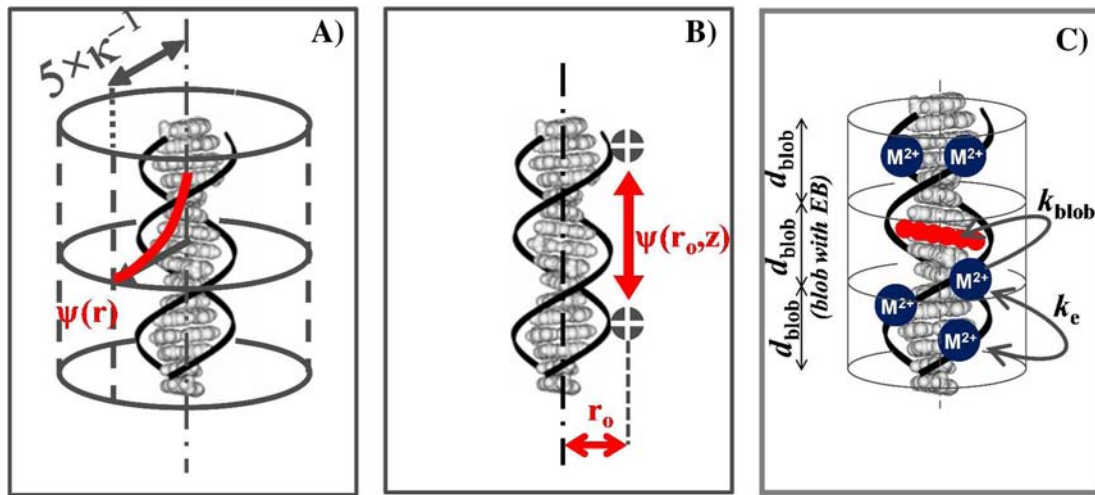


Figure 1. Representations of (A) the decay of the electrostatic potential $\psi(r)$ as a function of the distance r from the polyelectrolyte surface, (B) the electrostatic interactions controlling the distribution of counterions at the polyelectrolyte surface resulting from $\psi(r_0, z)$, and (C) the compartmentalization of the polyelectrolyte into *blobs* according to the fluorescence blob model. DNA-EB (oval shape) is intercalated at the center of the DNA duplex.⁵⁷ Inside a blob, DNA-EB is quenched by metal cations M^{2+} with a rate constant k_{blob} , while M^{2+} cations exchange between blobs with a rate constant k_e .⁵⁷

F-actin filaments that promote their self-aggregation into bundles.²²

While many experimental procedures have been implemented to provide information about $\psi(r)$ by determining the fraction of polyelectrolyte ions that are paired with counterions²³ or the composition of the ionic atmosphere surrounding a polyelectrolyte,²⁴ a much smaller number of experiments exist that describe $\psi(r_0, z)$ by directly probing the lateral distribution of counterions at the polyelectrolyte surface. With this in mind, this study presents a robust experimental procedure that provides the first measure of the length scale over which $\psi(r_0, z)$ affects the distribution of metal cations bound to DNA. DNA was chosen as a model polyelectrolyte to take advantage of the well-established relationship relating the length of a DNA scaffold with the number of base pairs (bp) that constitute it. Fluorescence spectroscopy was used to monitor the process of electron transfer that is known to take place from an excited ethidium bromide intercalated in DNA (DNA-EB) to Cu^{2+} and Ni^{2+} metal cations electrostatically bound to the DNA phosphates²⁵ and to determine the length scale over which metal cations distribute themselves around DNA. However, it must be noted that since the rate constant for electron transfer (k_{ET}) depends on the distance between the electron donor and the electron acceptor,^{26–37} using electron transfer to probe the distribution of metal cations randomly distributed around an excited DNA-EB represents a challenging task because the multiple distances separating each pair of DNA-EB and DNA-bound metal cation result in a distribution of k_{ET} values,^{25–45} which complicates the analysis of the fluorescence data. The introduction of metal-ligand complexes that can be covalently attached to specific positions of a DNA helix has provided an elegant means to control the distance over which electron transfer occurs.^{26–37,46–54} Unfortunately, this powerful procedure would have been of little use in the present study, which aimed to probe the process of electron transfer between DNA-EB and metal cations randomly distributed along the DNA helix. In this case, the fluorescence blob model (FBM) introduced by this laboratory in 1999 to probe the internal dynamics of randomly labeled linear polymers was used,^{55,56} as it has been shown to handle the complex kinetics induced by a

distribution of k_{ET} values for electron transfer between DNA-EB and DNA-bound metal cations.⁵⁷

Through the use of the FBM, the average distance over which electron transfer between an excited DNA-EB and DNA-bound metal cations occurs was found to equal the Debye length. The simplicity of this result should prove valuable to scientists interested in characterizing the complex behavior of polyelectrolytes, be they of biological or synthetic origin. As a case in point, this result was applied to rationalize the conformational changes undergone by a polyelectrolyte as a function of polyelectrolyte concentration and salt concentration.

RESULTS

Probing Electrostatic Interactions in DNA by Fluorescence Spectroscopy. The more than 10-fold enhancement in fluorescence lifetime and quantum yield experienced by ethidium bromide (EB) upon intercalation in DNA makes EB a well-suited marker to probe photophysical processes taking place at the DNA surface. Furthermore, excited DNA-EB has been reported to undergo efficient quenching upon oxidation by nearby Cu^{2+} or Ni^{2+} cations.²⁵ Consequently, the quenching of DNA-EB by metal cations bound to the DNA phosphates provides a convenient means to probe the distribution of metal cations bound to the DNA surface. As was previously demonstrated,⁵⁷ the random distribution of quenchers around the polyelectrolyte backbone and the associated distribution of quenching rate constants can be readily handled by applying the FBM to the analysis of the fluorescence decays acquired for aqueous solutions of DNA-EB and metal cations.

The FBM was introduced in 1999 to account for the complex kinetics induced by the formation of excimers between pyrene pendants randomly attached to a linear polymer.⁵⁵ The FBM acknowledges that the motion of an excited pyrene is restricted inside the polymer coil, as it needs to drag the chain segment to which it is covalently attached through the congested interior of the polymer coil. By recognizing that a pyrene probes a finite volume of the polymer coil called a *blob* while it remains excited, the polymer coil can be divided into a cluster of blobs

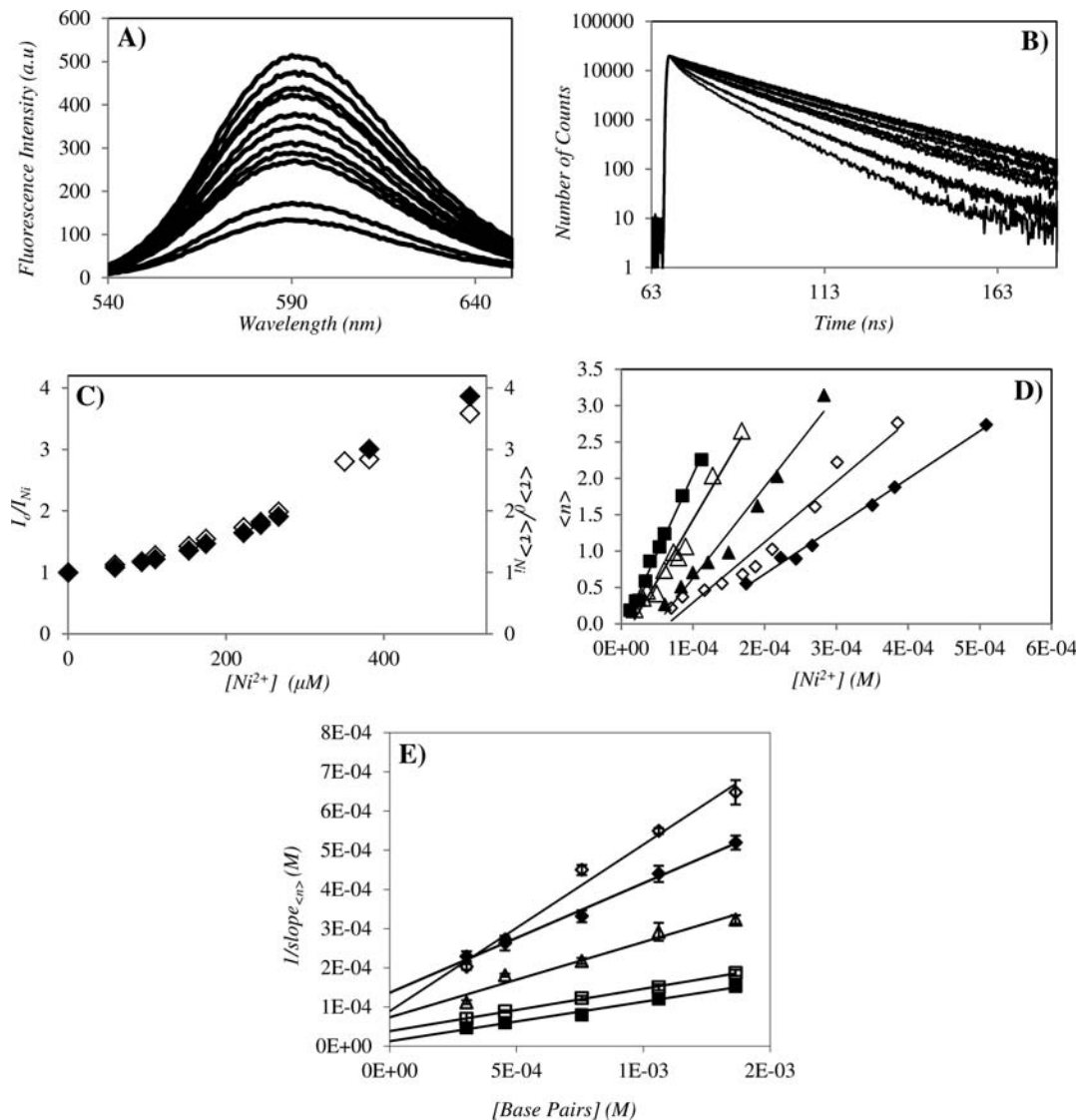


Figure 2. (A) Fluorescence spectra and (B) fluorescence decays of 1.36 mM calf thymus DNA solution with a NiCl_2 concentration ranging from (top to bottom) 0 to 5.09×10^{-4} M. (C) Corresponding Stern–Volmer plots obtained from steady-state (\blacklozenge) and time-resolved (\diamond) fluorescence ($\lambda_{\text{ex}} = 340$ nm, $\lambda_{\text{em}} = 605$ nm). (D) Plot of $\langle \tau \rangle$ vs Ni^{2+} concentration for DNA concentrations of 0.3 (\blacklozenge), 0.45 (\diamond), 0.76 (\blacktriangle), 1.05 (\triangle), and 1.36 mM (\blacksquare). (E) Plots of reciprocals of slopes of plots analogous to (D) vs DNA concentration with Na_2SO_4 concentrations of 3×10^{-2} (\diamond), 2×10^{-2} (\blacklozenge), 1.25×10^{-2} (\triangle), 5×10^{-3} (\square), and 5×10^{-4} M (\blacksquare). In (A–D), $[\text{EB}] = 1 \times 10^{-5}$ M and $[\text{Na}_2\text{SO}_4] = 5 \times 10^{-4}$ M.

among which the pyrenes randomly attached onto the polymer chain distribute themselves randomly according to a Poisson distribution. The time dependence of the concentration of excited pyrenes undergoing excimer formation can be derived by using mathematical procedures developed to handle identical kinetics taking place in micellar systems.⁵⁸ These derivations result in eq S2 in the Supporting Information (SI).^{55–58} Although the FBM was originally introduced to probe the dynamics of flexible polymers,^{55,56} where a blob made of a flexible polymer segment reflected de Gennes' definition of a polymer blob,⁵⁹ the same FBM has also been applied to study rigid double-stranded DNA⁵⁷ and α -helical poly(L-glutamic acid).^{60,61} In these examples, a blob represents a rigid segment of a polynucleotide⁵⁷ or polypeptide^{60,61} over which a photophysical process of interest such as electron transfer or pyrene excimer formation occurs. In the case of these rigid polymeric constructs, where a blob represents the cylinder surrounding a helical segment, the FBM refers more to

the general eq S2 in the SI rather than to de Gennes' original definition of a blob. In the case of quenching of DNA-EB via electron transfer to a metal cation, a blob represents a cylindrical volume centered around the stretch of DNA over which electron transfer takes place (see Figure 1C).

Figure 2A shows the fluorescence spectra of solutions of DNA-EB containing 1.36 mM DNA and 5×10^{-4} M Na_2SO_4 as increasing amounts of Ni^{2+} are added to the solution. Quenching by electron transfer is evident from the pronounced decrease in fluorescence intensity. The decrease in fluorescence intensity can be qualitatively described in terms of the ratio I_0/I , where I_0 and I represent the fluorescence intensities of DNA-EB without and with metal cations, respectively. The fluorescence decays were acquired for each solution, as shown in Figure 2B, and they exhibited an increased curvature at early times as more Ni^{2+} was added. The curved nature of the decays in Figure 2B reflects the distribution of quenching rate constants resulting from the random binding of the Ni^{2+} cations

onto DNA. The decays were first fit with a sum of exponentials according to eq S1 in the SI to determine the number-average decay time $\langle \tau \rangle$, and a measure of the quenching efficiency probed by time-resolved fluorescence measurements could be obtained from the ratio $\langle \tau \rangle_o / \langle \tau \rangle$, where $\langle \tau \rangle_o$ is the number-average lifetime of DNA-EB in the absence of metal cation. Plots of the ratios I_o/I and $\langle \tau \rangle_o / \langle \tau \rangle$ as functions of Ni^{2+} concentration (Figure 2C) display an upward curvature similar to that observed for surfactant micelles,⁶² which supports the notion that fluorescence quenching of DNA-EB via electron transfer occurs within a constrained geometry, as required for the application of the FBM to the analysis of the fluorescence decays.

Fitting the fluorescence decays in Figure 2B using eq S2 in the SI gave the average number of quenchers per blob, $\langle n \rangle$, which is plotted in Figure 2D as a function of Ni^{2+} concentration for all DNA concentrations used at a Na_2SO_4 concentration of 5×10^{-4} M. According to eq S4 in the SI, the parameter $\langle n \rangle$ represents a direct measure of the fraction of metal cations bound to DNA, as electron transfer is unlikely to occur efficiently between DNA-EB and unbound cations, as experiments carried out in an earlier publication demonstrate.⁵⁷ Consequently, the $\langle n \rangle$ values retrieved from FBM experiments reflect the condensation of cations along the DNA helix. After a certain onset value of the Ni^{2+} concentration ($[\text{M}^{2+}]_o$ in eq S4 in the SI), $\langle n \rangle$ increased linearly with increasing Ni^{2+} concentration ($[\text{M}^{2+}]_T$ in eq S7 in the SI). As explained in an earlier publication,⁵⁷ the onset concentration $[\text{M}^{2+}]_o$ results from a perturbation made to the electrostatic potential $\psi(r_o, z)$ at position $z = 0$, where a positively charged EB^+ is intercalated in the DNA duplex. The presence of EB^+ lowers the electrostatic potential locally around DNA-EB at $z = 0$, resulting in a $\psi(r_o, z = 0)$ value that is smaller in magnitude than $\psi(r_o, z \gg 0)$, the value of the electrostatic potential at positions $z \gg 0$ away from DNA-EB but still at the surface of the DNA helix, where $r = r_o$. This situation is illustrated in the top panel of Figure 3. Consequently, the metal cations prefer to bind to DNA away from DNA-EB at $z \gg 0$ (second panel of Figure 3), too far away from DNA-EB to induce electron transfer. As more metal cations are added to the solution, $\psi(r_o, z \gg 0)$ decreases in a discrete manner along the DNA duplex wherever metal cations bind, until its value matches that of

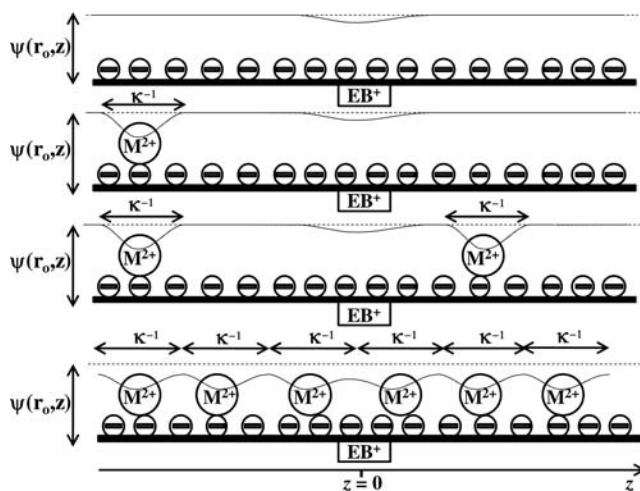


Figure 3. Predicted profile of the electrostatic potential $\psi(r_o, z)$ at the polyelectrolyte surface as counterions bind to the polyelectrolyte.

$\psi(r_o, z = 0)$; this occurs where the total concentration of metal cations, $[\text{M}^{2+}]_T$, equals the onset metal cation concentration $[\text{M}^{2+}]_o$ (bottom panel of Figure 3). For $[\text{M}^{2+}]_T$ concentrations greater than $[\text{M}^{2+}]_o$, binding of metal cations takes place close enough to DNA-EB for electron transfer to occur. As more metal cations bind to DNA, the blobs are progressively filled, and the average number of quenchers per blob increases linearly with $[\text{M}^{2+}]_T$, as found experimentally in Figure 2D.

As shown in the Experimental Section in the SI, the straight lines obtained in Figure 2D for $[\text{M}^{2+}]_T$ concentrations greater than $[\text{M}^{2+}]_o$ can be fitted with eq S7 in the SI. On the basis of this equation, the reciprocal of the slope of the straight lines in Figure 2D equals $(KN_{\text{blob}})^{-1} + N_{\text{blob}}^{-1}[\text{DNA}]$. Consequently, as shown in Figure 2E, plotting the reciprocal of the slope as a function of DNA concentration (expressed in units of moles of bp per liter) yields straight lines for the salt concentration of $[\text{Na}_2\text{SO}_4] = 5 \times 10^{-4}$ M used in Figure 2A–D and for all of the other Na_2SO_4 concentrations studied. On the basis of eq S8 in the SI, the slopes of the lines shown in Figure 2E equal N_{blob}^{-1} , which after multiplication by the height of a single bp (0.34 nm) gives d_{blob} , the average dimension of a blob.

Compartmentalization of Counterions along DNA into Blobs of Dimension κ^{-1} . A plot of d_{blob} as a function of salt concentration is shown in Figure 4. Surprisingly for a

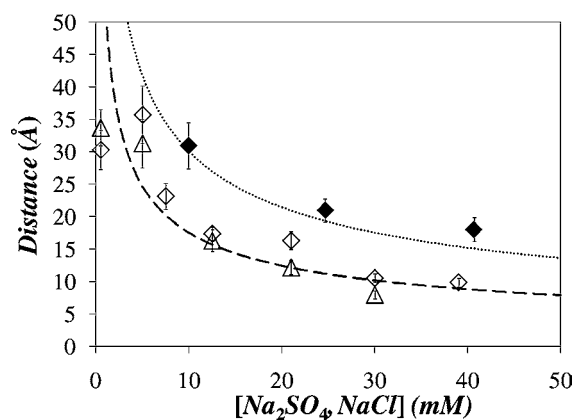


Figure 4. Plots of d_{blob} as functions of salt concentration obtained from fluorescence quenching measurements using Cu^{2+} (diamond) and Ni^{2+} (triangles). The open and solid symbols were obtained using Na_2SO_4 and NaCl , respectively, as the salt. The dashed and dotted lines represent κ^{-1} obtained with Na_2SO_4 and NaCl , respectively.

study based on electron transfer between an excited DNA-EB and two different metal cations, the trends obtained for d_{blob} with Ni^{2+} and Cu^{2+} in the presence of Na_2SO_4 overlapped within experimental error, indicating that the redox potential of the metal used in these experiments does not play a significant role for the range of salt concentrations studied. This observation was further reinforced by noting that d_{blob} obtained by fluorescence took values similar to the Debye length κ^{-1} , which depends solely on the ionic strength of the solution (see the dashed and dotted lines in Figure 4). Indeed, lowering the ionic strength of the solution by working with NaCl instead of Na_2SO_4 resulted in larger Debye lengths, which were matched nicely in Figure 4 by the d_{blob} values obtained by fluorescence.

Since d_{blob} is the length scale resulting ultimately from the interactions between DNA-EB and the metal cations that are controlled by electrostatic forces and the redox potential between the electron donor and acceptor, the trends shown in

Figure 4 demonstrate that κ^{-1} represents the limiting length scale probed by our experiments. Figure 3 provides a rationale for this result. As for EB⁺, binding of a metal cation M²⁺ to DNA induces a local dent in $\psi(r_o, z)$, which is decreased at the locus where M²⁺ is bound (second panel in Figure 3). Other M²⁺ cations tend to bind to DNA where $\psi(r_o, z)$ is strongest, that is, at distances d away from the first bound M²⁺ where $\psi(r_o, z)$ has recovered its original value. As the M²⁺ concentration is increased further, the crossover concentration [M²⁺]_o is reached, where M²⁺ ions bind at loci corresponding to a maximum of $\psi(r_o, z)$ by arranging themselves in a periodic array along DNA with a periodicity that is probed effectively by the FBM analysis over a length scale given by κ^{-1} as a first approximation.

The procedure described herein used DNA as a molecular ruler to relate N_{blob} to its equivalent distance d_{blob} and establish that d_{blob} is actually equal to κ^{-1} . The trends shown in Figure 4 represent a compilation of 745 fluorescence decays that were acquired and analyzed with the FBM. In view of the large number of experimental data that were rationalized with a single unifying analysis and the overall complexity of the system studied, with electron transfer processes occurring over multiple undefined distances along the DNA scaffold, the final result that $d_{blob} = \kappa^{-1}$ is remarkably straightforward. The data presented herein support the proposal that counterions bind to polyelectrolytes by distributing themselves according to a Poisson probability distribution into a periodic array of domains with dimensions equal to the Debye length (Figures 3 and 4). The compelling simplicity of this proposal can now be applied to rationalize some of the peculiar behaviors encountered with polyelectrolytes, such as the well-known but still poorly understood upshot in reduced viscosity observed for decreasing polyelectrolyte concentration in low-ionic-strength solvents.^{63–65}

DISCUSSION

The main implication conveyed by Figures 3 and 4 is that a charge on a polyelectrolyte feels neighboring charges over a distance equal to the Debye length (κ^{-1}). This distance corresponds to a segment of the polyelectrolyte that is locally rigid because neighboring charges repel each other. That first segment is flanked by two similar segments of length κ^{-1} that have no effect on the charges of the first segment. Consequently, these segments of length κ^{-1} can be viewed as independent rigid segments of the polyelectrolyte that can be used to evaluate the scaling laws that describe the dimension of polyelectrolytes in solution. Following Flory's formalism, the coil of the polyelectrolyte is expected to have a radius R_p whose scaling relationship with n , the number of segments of length κ^{-1} , is given in eq 1. The exponent ν is the Flory exponent, which equals 0.50 and 0.59 for neutral polymers in a θ solvent and a good solvent, respectively.⁵⁹

$$R_p \sim n^\nu \kappa^{-1} \quad (1)$$

If the polyelectrolyte is made of N monomers of dimension a , the number of segments n is equal to Na/κ^{-1} . Since the reduced viscosity η_{sp}/C (where C is the polymer concentration) is proportional to the volume of the polymer coil divided by N , the reduced viscosity scales as R_p^3/N ; thus, the reduced viscosity can be expressed by eq 2:

$$\frac{\eta_{sp}}{C} \sim \frac{\left(\frac{Na}{\kappa^{-1}}\right)^{3\nu} \kappa^{-3}}{N} = a^{3\nu} N^{3\nu-1} \kappa^{3(\nu-1)} \quad (2)$$

To evaluate ν , one uses the fact that according to Fuoss' equation, η_{sp}/C scales as $C^{-0.5}$ when no salt is added to the solution.⁶⁶ Since κ^{-1} also scales as $C^{-0.5}$ under those conditions, eq 2 implies that the exponent of κ , $3(\nu - 1)$, is equal to 1, which means that $\nu = 0.66$. This exponent is larger than the exponent of 0.59 obtained for neutral polymers in a good solvent, reflecting the stronger excluded volume effects induced by electrostatic repulsions between charged monomers. The exponent of 0.66 agrees quite well with the prediction of 0.634 reported in the literature for dilute polyelectrolyte solutions.⁶⁷ Indeed, using a Flory exponent of 0.66 appears to describe very well the high-polymer-concentration regime, where Fuoss' equation can be applied to the experimental trends of η_{sp}/C obtained for a series of partially sulfuric acid-esterified poly(vinyl alcohol)s as a function of C for different salt concentrations. This is shown in Figure 5, where κ^{-1} and η_{sp}/C

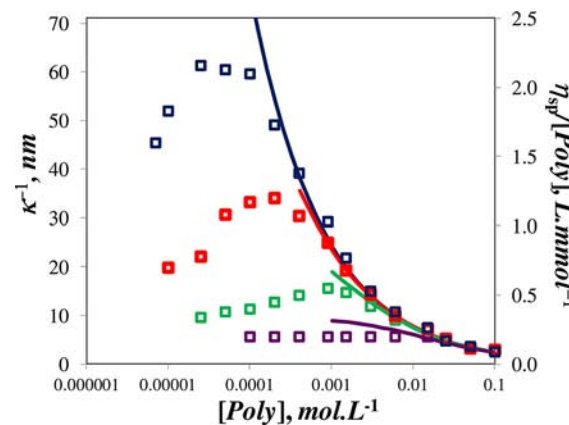


Figure 5. Plots of Debye length (κ^{-1} , lines, left axis) and reduced viscosity (η_{sp}/C , symbols, right axis) as functions of polymer concentration. Data were taken from ref 65 and were measured for partially sulfuric acid-esterified (31%) poly(vinyl alcohol) in water with $[NaCl] = 0$ mM (blue), 0.01 mM (red), 0.1 mM (green), and 1.0 mM (purple).

seem to behave in a similar manner in the region of large polymer concentration of the plot.⁶³ Equation 2 also predicts that for a given value of κ^{-1} , η_{sp}/C which scales as $N\kappa^{-1}$ increases linearly with increasing molecular weight, as has been observed experimentally.⁶⁴ Equation 1 predicts that as the polymer concentration decreases, R_p should increase as $N^2\kappa^{-1}$, and eq 2 holds as long as n , the number of segments of dimension κ^{-1} , is much larger than unity, at which point the polyelectrolytes can be viewed as extended rods that interact strongly in solution, resulting in the maximum value of η_{sp}/C . Further diluting the polymer solution past this point reduces the strong electrostatic interactions between polyelectrolytes, resulting in the precipitous drop in η_{sp}/C at low polymer concentration.

CONCLUSIONS

Quenching of DNA-EB by electron transfer to Cu²⁺ and Ni²⁺ cations was characterized by time-resolved fluorescence spectroscopy. By analysis of no less than 745 fluorescence decays with the FBM and processing of this large data set through the same protocol outlined in the Experimental Section in the SI,

the blob size over which electron transfer occurred was determined as a function of salt concentration for two salts, namely, NaCl and Na₂SO₄. The size of a cylindrical blob, given by its height d_{blob} as described in Figure 1C, was found to match closely the Debye length as a function of the ionic strength of the solution, as shown in Figure 4. Also, little difference was observed whether Cu²⁺ or Ni²⁺ cations were used in these experiments. This observation further supports the notion that electron transfer is controlled by the distribution of the cations around DNA-EB rather than the redox potential of the species involved. In view of the complexity of the system at hand, the simplicity of this final result is fascinating. Indeed, electron transfer took place over a distribution of distances, and thus a distribution of rate constants, as DNA-EB and metal cations were randomly bound to DNA. Nevertheless, the FBM formalism based on a small set of parameters could describe the decays rather well, and interpretation of these parameters retrieved from the analysis was straightforward and illustrated how counterions bind to a polyelectrolyte.

Our fluorescence quenching experiments suggest that counterions bind to a polyelectrolyte by distributing themselves according to a Poisson probability distribution among independent compartments made of polyelectrolyte segments of length κ^{-1} . Because this length scale describes the distribution of counterions at the DNA surface along the DNA axis (where $r = r_o$; see Figures 1 and 3), it is different in nature from most other length scales that have been introduced in the literature to describe the decrease in the electrostatic potential of DNA in the radial direction away from the DNA axis for distances $r > r_o$. For instance, the electrostatic potential of DNA, $\psi(r > r_o, z)$, decreases exponentially with increasing r as $\exp(-kr)$ for an isolated DNA helix in solution.⁶ For DNA helices in dense DNA aggregates or dense complexes made of DNA and cationic lipids, the helical pitch of DNA is introduced to define short length scales equal to, respectively, $0.5(\kappa^{-1} + g^2)^{-1/2}$, where g is the reciprocal of the pitch (0.176 Å⁻¹ for B-DNA), and $(\kappa^{-1} + ng^2)^{-1/2}$, where n is an integer, over which repulsive and attractive forces take place between different DNA helices.^{17,18} As the properties of polyelectrolytes in dilute solution or in dense aggregates depend on the binding of counterions,^{5–9} our conclusion that the binding of counterions to DNA occurs over a length scale given by κ^{-1} is expected to have far-reaching implications. As a case in point, our result seems to provide a self-consistent framework for describing the complex behavior of polyelectrolytes in solution.

ASSOCIATED CONTENT

Supporting Information

Experimental section and tables with all parameters retrieved from the analysis of the fluorescence decays, the slopes and intercepts for the lines obtained by plotting $\langle n \rangle$ versus metal cation concentration, and all N_{blob} and K values. This material is available free of charge via the Internet at <http://pubs.acs.org>.

AUTHOR INFORMATION

Corresponding Author

jduhamel@uwaterloo.ca

Notes

The authors declare no competing financial interest.

ACKNOWLEDGMENTS

The authors gratefully acknowledge generous support from the Natural Sciences and Engineering Research Council of Canada, the Canadian Foundation for Innovation, and a Premier Research Excellence Award of Ontario.

REFERENCES

- (1) Kreth, G.; Finsterle, J.; von Hase, J.; Cremer, M.; Cremer, C. *Biophys. J.* **2004**, *86*, 2803–2812.
- (2) Koltover, I.; Salditt, T.; Rädler, J. O.; Safinya, C. R. *Science* **1998**, *281*, 78–81.
- (3) Decher, G. *Science* **1997**, *277*, 1232–1237.
- (4) Jager, E. W. H.; Inganäs, O.; Lundström, I. *Science* **2000**, *288*, 2335–2338.
- (5) Wong, G. C. L.; Pollack, L. *Annu. Rev. Phys. Chem.* **2010**, *61*, 171–189.
- (6) Messina, R. *J. Phys.: Condens. Matter* **2009**, *21*, No. 113102.
- (7) Cherstvy, A. G. *Phys. Chem. Chem. Phys.* **2011**, *13*, 9942–9968.
- (8) Kornyshev, A. A.; Lee, D. J.; Leikin, S.; Wynveen, A. *Rev. Mod. Phys.* **2007**, *79*, 943–996.
- (9) Kornyshev, A. A. *Phys. Chem. Chem. Phys.* **2010**, *12*, 12352–12378.
- (10) Manning, G. S. *J. Chem. Phys.* **1969**, *51*, 924–933.
- (11) Manning, G. A. *J. Chem. Phys.* **1969**, *51*, 934–938.
- (12) Manning, G. S. *J. Chem. Phys.* **1969**, *51*, 3249–3252.
- (13) Manning, G. S. *Q. Rev. Biophys.* **1978**, *11*, 179–246.
- (14) Deserno, M.; Holm, C.; May, S. *Macromolecules* **2000**, *33*, 199–206.
- (15) Deserno, M.; Holm, C. *Mol. Phys.* **2002**, *100*, 2941–2956.
- (16) Wagner, K.; Keyes, E.; Kephart, T. W.; Edwards, G. *Biophys. J.* **1997**, *73*, 21–30.
- (17) Kornyshev, A. A.; Leikin, S. *J. Chem. Phys.* **1997**, *107*, 3656–3674.
- (18) Kornyshev, A. A.; Leikin, S. *Phys. Rev. Lett.* **1999**, *82*, 4138–4141.
- (19) Cherstvy, A. G. *J. Phys. Chem. B* **2010**, *114*, 5241–5249.
- (20) Cherstvy, A. G.; Kornyshev, A. A. *J. Phys. Chem.* **2005**, *109*, 13024–13029.
- (21) Cherstvy, A. G. *J. Phys. Chem. B* **2007**, *111*, 7914–7927.
- (22) Angelini, T. E.; Liang, H.; Wriggers, W.; Wong, G. C. L. *Proc. Natl. Acad. Sci. U.S.A.* **2003**, *100*, 8634–8637.
- (23) Morishima, Y.; Nomura, S.; Ikeda, T.; Seki, M.; Kamachi, M. *Macromolecules* **1995**, *28*, 2874–2881.
- (24) Bai, Y.; Greenfeld, M.; Travers, K. J.; Chu, V. B.; Lipfert, J.; Doniach, S.; Herschlag, D. *J. Am. Chem. Soc.* **2007**, *129*, 14981–14988.
- (25) Atherton, S. J.; Beaumont, P. C. *J. Phys. Chem.* **1986**, *90*, 2252–2259.
- (26) Grinstaff, M. W. *Angew. Chem., Int. Ed.* **1999**, *38*, 3629–3635.
- (27) Turro, N. J.; Barton, J. K. *J. Biol. Inorg. Chem.* **1998**, *3*, 201–209.
- (28) Maiya, B. G.; Ramasarma, T. *Curr. Sci.* **2001**, *80*, 1523–1530.
- (29) Lewis, F. D.; Wu, Y. *J. Photochem. Photobiol., C* **2001**, *2*, 1–16.
- (30) Lewis, F. D.; Letsinger, R. L. *J. Biol. Inorg. Chem.* **1998**, *3*, 215–221.
- (31) Lewis, F. D.; Liu, X.; Wu, Y.; Miller, S. E.; Wasielewski, M. R.; Letsinger, R. L.; Sanishvili, R.; Joachimiak, A.; Tereshko, V.; Egli, M. *J. Am. Chem. Soc.* **1999**, *121*, 9905–9906.
- (32) Lewis, F. D.; Taifeng, W.; Zhang, Y.; Letsinger, R. L.; Greenfield, S. R.; Wasielewski, M. R. *Science* **1997**, *277*, 673–676.
- (33) Siegmund, K.; Daublain, P.; Wang, Q.; Trifonov, A.; Feibig, T.; Lewis, F. D. *J. Phys. Chem. B* **2009**, *113*, 16276–16284.
- (34) Fukui, K.; Tanaka, K.; Fujitsuka, M.; Watanabe, A.; Ito, O. *J. Photochem. Photobiol., B* **1999**, *50*, 18–27.
- (35) Fukui, K.; Tanaka, K. *Angew. Chem., Int. Ed.* **1998**, *37*, 158–161.
- (36) Wan, C.; Feibig, T.; Kelley, S. O.; Treadway, C. R.; Barton, J. K.; Zewail, A. H. *Proc. Natl. Acad. Sci. U.S.A.* **1999**, *96*, 6014–6019.
- (37) Kelley, S. O.; Holmlin, E.; Stemp, E. D. A.; Barton, J. K. *J. Am. Chem. Soc.* **1997**, *119*, 9861–9870.
- (38) Prusik, T.; Geacintov, N. E. *FEBS Lett.* **1976**, *71*, 236–240.

- (39) Atherton, S. J.; Beaumont, P. C. *J. Phys. Chem.* **1987**, *91*, 3993–3997.
- (40) Atherton, S. J.; Beaumont, P. C. *J. Phys. Chem.* **1995**, *99*, 12025–12029.
- (41) Baguley, B. C.; Le Bret, M. *Biochemistry* **1984**, *23*, 937–943.
- (42) Fromherz, P.; Rieger, B. *J. Am. Chem. Soc.* **1986**, *108*, 5361–5362.
- (43) Brun, A. M.; Harriman, A. *J. Am. Chem. Soc.* **1992**, *114*, 3656–3660.
- (44) Harriman, A. *Angew. Chem., Int. Ed.* **1999**, *38*, 945–949.
- (45) Arkin, M. R.; Stemp, E. D. A.; Holmlin, R. E.; Barton, J. K.; Hormann, A.; Olson, E. J. C.; Barbara, P. F. *Science* **1996**, *273*, 475–480.
- (46) Wagenknecht, H.-A. *Charge Transfer in DNA: From Mechanism to Application*; Wiley- VCH: Weinheim, Germany, 2005.
- (47) Murphy, C. J.; Arkin, M. R.; Jenkins, Y.; Ghatlia, N. D.; Bossmann, S. H.; Turro, N. J.; Barton, J. K. *Science* **1993**, *262*, 1025–1029.
- (48) Gorodetsky, A. A.; Buzzeo, M. C.; Barton, J. K. *Bioconjugate Chem.* **2008**, *19*, 2285–2296.
- (49) Augustyn, K. E.; Stemp, E. D. A.; Barton, J. K. *Inorg. Chem.* **2007**, *46*, 9337–9350.
- (50) Valis, L.; Wang, Q.; Raytchev, M.; Buchvarov, I.; Wagenknecht, H.-A.; Fiebig, T. *Proc. Natl. Acad. Sci. U.S.A.* **2006**, *103*, 10192–10195.
- (51) Hall, D. B.; Kelley, S. O.; Barton, J. K. *Biochemistry* **1998**, *37*, 15933–15940.
- (52) Shao, F.; Barton, J. K. *J. Am. Chem. Soc.* **2007**, *129*, 14733–14738.
- (53) Kelley, S. O.; Barton, J. K. *Science* **1999**, *283*, 375–381.
- (54) Krider, E. S.; Meade, T. J. *J. Biol. Inorg. Chem.* **1998**, *3*, 222–225.
- (55) Mathew, A.; Siu, H.; Duhamel, J. *Macromolecules* **1999**, *32*, 7100–7108.
- (56) Duhamel, J. *Acc. Chem. Res.* **2006**, *39*, 953–960.
- (57) Keyes Baig, C.; Duhamel, J. *J. Phys. Chem. B* **2010**, *114*, 13950–13960.
- (58) Tachiya, M. *Chem. Phys. Lett.* **1975**, *33*, 289–292.
- (59) De Gennes, P.-G. In *Scaling Concepts in Polymer Physics*; Cornell University Press: Ithaca, NY, 1979.
- (60) Duhamel, J.; Kanagalingam, S.; O'Brien, T.; Ingratta, M. *J. Am. Chem. Soc.* **2003**, *125*, 12810–12822.
- (61) Ingratta, M.; Duhamel, J. *J. Phys. Chem. B* **2008**, *112*, 9209–9218.
- (62) Turro, N. J.; Yekta, A. *J. Am. Chem. Soc.* **1978**, *100*, 5951–5952.
- (63) Nishida, K.; Kaji, K.; Kanaya, T.; Fanjat, N. *Polymer* **2002**, *43*, 1295–1300.
- (64) Cohen, J.; Priel, Z.; Rabin, Y. *J. Chem. Phys.* **1988**, *88*, 7111–7116.
- (65) Jousset, S.; Bellissent, H.; Galin, J. C. *Macromolecules* **1998**, *31*, 4520–4530.
- (66) Fuoss, R. *M. J. Polym. Sci.* **1948**, *3*, 603–604.
- (67) Chitanvis, S. M. *Phys. Rev. E* **2003**, *68*, No. 061802.